

# Relationship between tooth macrowear and jaw morphofunctional traits in hypercarnivores (#104882)

1

First submission

## Guidance from your Editor

Please submit by **22 Sep 2024** for the benefit of the authors (and your token reward) .



### Structure and Criteria

Please read the 'Structure and Criteria' page for guidance.



### Raw data check

Review the raw data.



### Image check

Check that figures and images have not been inappropriately manipulated.

If this article is published your review will be made public. You can choose whether to sign your review. If uploading a PDF please remove any identifiable information (if you want to remain anonymous).

## Files

Download and review all files from the [materials page](#).

7 Figure file(s)

2 Table file(s)

1 Raw data file(s)




# Structure and Criteria

## Structure your review

The review form is divided into 5 sections. Please consider these when composing your review:

1. BASIC REPORTING
2. EXPERIMENTAL DESIGN
3. VALIDITY OF THE FINDINGS
4. General comments
5. Confidential notes to the editor






 You can also annotate this PDF and upload it as part of your review

When ready [submit online](#).





## Editorial Criteria

Use these criteria points to structure your review. The full detailed editorial criteria is on your [guidance page](#).




### BASIC REPORTING

-  Clear, unambiguous, professional English language used throughout.
-  Intro & background to show context. Literature well referenced & relevant.
-  Structure conforms to [Peerj standards](#), discipline norm, or improved for clarity.
-  Figures are relevant, high quality, well labelled & described.
-  Raw data supplied (see [Peerj policy](#)).

### EXPERIMENTAL DESIGN

-  Original primary research within [Scope of the journal](#).
-  Research question well defined, relevant & meaningful. It is stated how the research fills an identified knowledge gap.
-  Rigorous investigation performed to a high technical & ethical standard.
-  Methods described with sufficient detail & information to replicate.

### VALIDITY OF THE FINDINGS

-  **Impact and novelty is not assessed.** Meaningful replication encouraged where rationale & benefit to literature is clearly stated.
-  All underlying data have been provided; they are robust, statistically sound, & controlled.
-  Conclusions are well stated, linked to original research question & limited to supporting results.



The best reviewers use these techniques

## Tip

## Example

**Support criticisms with evidence from the text or from other sources**

*Smith et al (J of Methodology, 2005, V3, pp 123) have shown that the analysis you use in Lines 241-250 is not the most appropriate for this situation. Please explain why you used this method.*

**Give specific suggestions on how to improve the manuscript**

*Your introduction needs more detail. I suggest that you improve the description at lines 57- 86 to provide more justification for your study (specifically, you should expand upon the knowledge gap being filled).*

**Comment on language and grammar issues**

*The English language should be improved to ensure that an international audience can clearly understand your text. Some examples where the language could be improved include lines 23, 77, 121, 128 – the current phrasing makes comprehension difficult. I suggest you have a colleague who is proficient in English and familiar with the subject matter review your manuscript, or contact a professional editing service.*

**Organize by importance of the issues, and number your points**

1. Your most important issue
2. The next most important item
3. ...
4. The least important points

**Please provide constructive criticism, and avoid personal opinions**

*I thank you for providing the raw data, however your supplemental files need more descriptive metadata identifiers to be useful to future readers. Although your results are compelling, the data analysis should be improved in the following ways: AA, BB, CC*

**Comment on strengths (as well as weaknesses) of the manuscript**

*I commend the authors for their extensive data set, compiled over many years of detailed fieldwork. In addition, the manuscript is clearly written in professional, unambiguous language. If there is a weakness, it is in the statistical analysis (as I have noted above) which should be improved upon before Acceptance.*

# Relationship between tooth macrowear and jaw morphofunctional traits in hypercarnivores

Jack Tseng<sup>Corresp., 1, 2</sup>, Larisa DeSantis<sup>3</sup>

<sup>1</sup> University of California, Berkeley, Berkeley, United States

<sup>2</sup> American Museum of Natural History, New York, United States

<sup>3</sup> Vanderbilt University, Nashville, United States

Corresponding Author: Jack Tseng

Email address: zjt@berkeley.edu

The mammalian adult dentition is a non-renewable resource. Tooth attrition and disease must be accommodated by ~~individuals~~ using behavioral, physiological, and/or musculoskeletal shifts to minimize impact on masticatory performance. From a biomechanical perspective, the musculoskeletal system becomes less efficient at producing bite force for a given amount of muscle input force over an individual's life, because tooth-food contact area increases as cusps wear. In this study we ask the question: does mandibular biomechanical performance show evidence of compensation with increasing tooth wear? We use three carnivoran ecomorphologies (meat specialist, scavenger, bone cracker) as a study system to compare morphofunctional data on tooth macrowear, jaw depth, bite mechanical efficiency, and jaw stress during biting. No significant shifts in adult mandibular corpus dimensions occurs in the sampled taxa as canine and carnassial teeth wear. In bone crackers carnassial biting mechanical efficiency increases significantly with increasing tooth wear, with no significant change in mandibular stress. Analyses of the fossil carnivore *Hyaenodon* suggests an increase in canine biting efficiency with increased tooth wear, but this may reflect interspecific variation rather than a life history one. Overall, these findings indicate that scavengers and meat specialists do not exhibit morphofunctional compensation for the decreased mechanical capability of worn and dull teeth. Behavioral modifications, rather than musculoskeletal adjustments, may instead play a major role in maintaining food ~~acquisition~~ and processing capabilities for individuals surviving into advanced ontogenetic age and tooth wear. These observations highlight the mammalian masticatory system as having a dynamic performance profile through its useful lifespan, and encourage a more nuanced understanding of past and present carnivore guilds by considering wear-dependent performance changes as a possible source of selection.

# Relationship between tooth macrowear and jaw morphofunctional traits in hypercarnivores

Z. Jack Tseng<sup>1,2</sup> and Larisa DeSantis<sup>3</sup>

<sup>1</sup> Department of Integrative Biology and Museum of Paleontology, University of California, Berkeley, California, United States of America

<sup>2</sup> Division of Paleontology, American Museum of Natural history, New York, New York, United States of America

<sup>3</sup> Department of Biological Sciences and Department of Earth and Environmental Sciences, Vanderbilt University, Nashville, Tennessee, United States of America

Corresponding Author:

Z. Jack Tseng<sup>1</sup>

Department of Integrative Biology and Museum of Paleontology, University of California, Berkeley, California, United States of America

Email address: [zjt@berkeley.edu](mailto:zjt@berkeley.edu)

# Abstract

The mammalian adult dentition is a non-renewable resource. Tooth attrition and disease must be accommodated by ~~individuals~~ using behavioral, physiological, and/or musculoskeletal shifts to minimize impact on masticatory performance. From a biomechanical perspective, the musculoskeletal system becomes less efficient at producing bite force for a given amount of muscle input force over an individual's life, because tooth-food contact area increases as cusps wear. In this study we ask the question: does mandibular biomechanical performance show evidence of compensation with increasing tooth wear? We use three carnivoran ecomorphologies (meat specialist, scavenger, bone cracker) as a study system to compare morphofunctional data on tooth macrowear, jaw depth, bite mechanical efficiency, and jaw stress during biting. No significant shifts in adult mandibular corpus dimensions occurs in the sampled taxa as canine and carnassial teeth wear. In bone crackers carnassial biting mechanical efficiency increases significantly with increasing tooth wear, with no significant change in mandibular stress. Analyses of the fossil carnivore *Hyaenodon* suggests an increase in canine biting efficiency with increased tooth wear, but this may reflect interspecific variation rather than a life history one. Overall, these findings indicate that scavengers and meat specialists do not exhibit morphofunctional compensation for the decreased mechanical capability of worn and dull teeth. Behavioral modifications, rather than musculoskeletal adjustments, may instead play a major role in maintaining food ~~acquisition~~ and processing capabilities for individuals surviving into advanced ontogenetic age and tooth wear. These observations highlight the mammalian masticatory system as having a dynamic performance profile through its useful lifespan, and encourage a more nuanced understanding of past and present carnivore guilds by considering wear-dependent performance changes as a possible source of selection.

# Introduction

Diphyodonty, the condition of having two generations of teeth throughout an individual's life, is a salient feature of crown mammals (Luo, Kielan-Jaworoska & Cifelli, 2004). Evolutionary benefits of having a permanent or adult set of dentitions may include functional consistency and stability in support of heterodonty, maintenance of precise occlusal performance, and reduction of energetic budget spent on dental growth. However, a principal trade-off of diphyodonty is the constraint of the permanent dentition as a non-renewable tissue. Wear or breakage to the adult teeth may affect their function, and any performance compensation in response must be made from other parts of the masticatory system because tooth enamel cannot repair itself. The evolutionary manifestation of this key property of mammalian dental tissues can be observed in species ranging from shrews to elephants, in which tooth wear severity is a limiting factor in individual lifespans (Lucas & van Casteren, 2014).

A concomitant evolutionary innovation alongside a diphyodont and heterodont dentition in mammals is a many-to-one form-function linkage of their lower jaws. The post-KPg radiation of mammalian taxonomic diversity also reflects a radiation of jaw shape disparity (Tseng et al., 2023). However, jaw biomechanical performance, specifically stiffness, is both elevated and less variable in crown mammals than in other vertebrates. This suggests that a stiff jaw is a synapomorphic condition of crown mammals regardless of feeding ecology.

The combination of a stiff lower jaw bone and a diphyodont, heterodont dentition underlies the diversity of feeding ecologies observed across living mammals (Jones et al., 2009). Although tooth wear and its corresponding functional changes is a fact of life for most mammals, it is

unclear whether the universally stiff jaws of mammals compared to other vertebrates implies that overall biting biomechanical performance is maintained across mammalian tooth wear stages. The amount of pressure or stress that can be generated at the tooth-food contact surface is inversely proportional to the area of that contact; for a given amount of force generated, stress is equal to that force divided by the area through which the force is applied. For resistant food items that require crushing, cracking, or shearing, the most efficient way to generate a fracture in the food bolus is to concentrate the bite force over a small occlusal area of the tooth crown. As teeth wear, the occlusal area enlarges, and thus the same masticatory task would require higher forces to generate the same pressure/stress at the tooth-food interface. Again, because tooth enamel wear is irreversible, any compensation to biting performance must come from elsewhere in the masticatory system.

In this study, we ask whether the lower jaw exhibits different morphofunctional characteristics according to the severity of tooth wear. We also ask whether any such morphofunctional traits support the identification of convergent feeding ecologies in the fossil record. We use a carnivoran study system, well-known for its strong link between tooth wear and feeding ecology (DeSantis et al., 2015; DeSantis, 2016; Burt & DeSantis, 2022), to test two hypotheses:

H<sub>1</sub>: Bone cracking and scavenging ecological morphologies (ecomorphs; Werdelin & Gittleman, 1996; Van Valkenburgh, 2007), representing mechanically demanding diets, exhibit morphofunctional compensation of decreased force to area ratio for a given input muscle force as tooth wear increases; there should be a significant difference in mechanical efficiency, strain energy, and/or jaw dimensions across tooth macrowear categories. By contrast, meat specialists,



which do not experience high mechanical demands, do not exhibit morphofunctional compensation for tooth wear.

H<sub>2</sub>: The fossil taxon *Hyaenodon*, long interpreted as ecological avatars of hyenas, should exhibit similar relationships between tooth macrowear and morphofunctional trait variation as extant bone cracking and scavenging ecomorphs represented by hyenas. Such similarity reflects similar ecomorphological adaptation between *Hyaenodon* and extant hyaenids.

## Materials & Methods

All morphofunctional data analyzed in this study are based on 2D photographs of hemimandible specimens in two museum collections: the American Museum of Natural History (AMNH) and the University of Michigan Museum of Zoology (UMMZ). A total of 54 specimens representing six genera were included in the analyses (Table 1). Each AMNH specimen was placed onto the scanning area of a Dell AIO A960 Flatbed Scanner in its natural resting position with the lateral side facing the scanning bed. A metric scale bar was placed next to the specimen. A color image at a resolution 600 dpi was then captured and saved as a tiff image file. UMMZ specimen images were downloaded from the Animal Diversity Web (<https://animaldiversity.org>) under an CC BY-NC-SA 3.0 license by P. Myers.

**Tooth macrowear analysis.** We categorized wear stages of all canine and carnassial teeth in the dataset using the scheme defined in DeSantis et al. (2017). Each tooth was given a score from 1 to 3, where a score of 1 indicates little to no occlusal wear with little or no dentine exposed, 2

indicates moderate occlusal wear with dentine exposure, and 3 indicates extensive occlusal wear with dentine exposure larger in area than the remaining enamel at the wear surface.

**Jaw measurements.** We used FIJI (Goldstein et al., 2018) to take all linear measurements. Each image was opened in FIJI, calibrated by setting the scale according to the length of 10 mm on the scale bar included in each photograph, and then using the line tool to make measurements. Jaw length measurements were taken on all specimens by taking the distance between the anterior boundary of the first lower incisor and the mandibular bone, and the posterior-most point on the condylar process. Two additional measurements were taken as proxies for the bending strength of the mandibular ramus below canine and carnassial bite positions, respectively: depth of ramus at the post-carnassial position, and depth of ramus at the post-canine position. Lastly, we record total jaw model volume from the finite element models of each specimen, the construction of which is detailed below.

**Biomechanical performance estimates (Fig. 1).** Each specimen image was converted into a high contrast image that represents the jaw in black pixels and surrounding space in white pixels. We used the magnetic lasso tool in GIMP 2.10.20 to select the jaw, reversed the object selection, and removed background pixels. The high contrast image was then exported as .png files and next converted into an outline bound by nodes within Inkscape version 0.48. The outlines were saved as .dxf files. Next, the outline shape was extruded with an arbitrary thickness of height 10 using OpenSCAD version 2014.01.29 and converted into a mesh file in .stl format. The extruded shape was then improved for triangular element count, aspect ratio, and evenness in Geomagic Wrap 2019. The imported stl meshes were first refined to represent at least 60k triangular faces,

then cleaned using the ‘quick smooth’ tool. The meshes were then decimated to a target triangle face count of 50k, with triangle face dimensional aspect ratio constrained to 10 or less. Lastly, the meshes were subjected to the mesh improvement tool ‘mesh doctor’ and then alternated with mesh decimation until the mesh improvement tool no longer detected any mesh issues. The final clean meshes were then exported as stl files and used for 2D finite element modeling.

We used Strand7 finite element analysis software version 2.4.6 to estimate biomechanical performance traits from the extruded mandibular meshes. Meshes were checked and cleaned using the automatic clean mesh tool in Strand7. If errors were detected during this mesh cleaning step, the mesh was taken through the improvement procedure outlined in the previous paragraph and reimported into Strand7 until no errors were detected. The mesh file was then exported once again as stl files for muscle and tooth enamel mesh generation.

The vetted mesh file from Strand7 was then reimported into Geomagic Wrap to generate muscle and tooth enamel mesh groups. Three muscle groups were delineated on the ascending ramus of the jaw shape based on previous descriptions of musculoskeletal anatomy in spotted hyenas (Tseng & Binder, 2010) and carnivorans in general (Evans & Christensen, 1979; Tseng & Stynder, 2011). The temporalis, superficial masseter, and deep masseter muscles were included in the biting simulation models; given the 2D approach, muscles that largely contribute to lateral jaw movements such as pterygoideus muscles were not modeled. The enamel crown of the canine and cheek dentitions on the mesh models were highlighted based on the enamel crown areas visible from specimen photographs. The highlighted triangle faces were then copied and

pasted as a separate mesh group to allow different material properties to be defined during the model simulation step (see below).

Photographs of cranial specimens for all six genera included in the analyses were used to generate reference cranial meshes using the same protocol described above for mandible mesh generation. The reference cranial meshes (one for each genus) were then imported and scaled to each mandible mesh for mandibular muscle force contraction vector estimation. We scaled the cranial reference to each mandible mesh by aligning the dorsal face of the mandible condyle with the ventral face of the mandibular fossa on the temporal bone, and the distal face of the lower canine tooth to the mesial face of the upper canine tooth, respectively. The cranial reference mesh was then rotated away from the mandible mesh by 30 degrees, representing an average gape for carnivorans (Bourke et al., 2008). Next, centroid points were generated for each of the three muscle groups. Muscle origination areas were highlighted on the cranial reference mesh, extruded to a thickness of 1 mm, and a ‘center of mass’ point was calculated using the function of the same name in Geomagic Wrap. These 3D centroid points were used as a reference to create 2D centroid coordinates directly on the surface of the original 2D muscle highlights. The x and y values of the centroid coordinates were recorded for each jaw-cranial mesh combination.

Next, muscle forces, joint and bite point constraints, and material properties were defined to fully parameterize the jaw model. The amount of force generated by each muscle insertion area (towards the centroid points on cranial reference meshes) was set to be proportional to the surface area represented by the muscle insertion meshed, multiplied by 0.3 N based on a maximum muscle contraction force of 0.3 N/mm<sup>2</sup> (Wroe, McHenry & Thomason, 2005). We

used muscle insertion area as a proxy for muscle contractile force rather than estimated physiological cross section area because 3D information is not available from the 2D specimen photographs. It is important to note that the underlying assumption of our approach is that muscle insertion area is a good approximation of its force production capability. We argue that this is a reasonable assumption, as it standardizes our interspecific comparisons of biomechanical response to biting scenarios as a product of overall muscle contraction rather than species-specific muscle activation ratios, for which no empirical data are available.

We used the BoneLoad program (Grosse et al., 2007) to generate distributed force vectors over muscle insertion areas to mimic muscle contraction. The force loaded meshes were then reimported into Strand7, where free body movement constraints and material properties were defined. Although all parts of the jaw model are represented by 2D plate elements, we defined a thick of 10% of the maximum model length to enable calculation of in-plane bending stress. A negligible thickness of 0.0001 mm was assigned to muscle attachment meshes to simulate the direct action of muscle fibers pulling on the underlying bone. Young's (elastic) modulus of 20 GPa (gigapascals) and Poisson ratio of 0.3 were assigned to the bone and muscle portions of the mesh model. The tooth enamel portion of the model was assigned a modulus of 20 GPa and Poisson ratio of 0.3.

Three different bite scenarios were simulated: canine bite, canine pull, and carnassial (m1 in carnivorans, m3 in *Hyaenodon*) bite (Fig. 1). In all three cases we placed a full nodal constraint at the center of the condylar process that prevented any translational or rotational movement. In the canine bite scenario, a partial nodal constraint was placed at the tip of the canine tooth to

prevent dorsoventral movement but allowing anteroposterior movement. This scenario simulated full muscle contraction during jaw closure and food contact at the tip of the canine. In the canine pull scenario, an anteriorly direct force equivalent to 10% of total muscle input force was placed at the same canine constraint as in the canine bite scenario, and all other conditions are identical to the canine bite scenario. This scenario simulated full muscle contraction during jaw closure, with a bite point at the canine and an external force from struggling prey. Lastly, in the carnassial bite scenario, the jaw joint constraint is as in the other two scenarios, but a cusp nodal constraint is placed at the carnassial paraconid instead of the canine tooth. This scenario simulated jaw closure with full muscle contraction during mastication at the carnassial tooth.

All three bite scenarios were solved using Strand7's linear static solver function. We then extracted both qualitative and quantitative data from the three bite scenarios. Output nodal reaction forces at the tooth cusp constraints were measured for the canine and carnassial bite scenarios and divided by total input muscle force to derive mechanical efficiency. Stored strain energy (in Joules), a measure of the work done by an input load in deforming a structure under load given a set of constraint conditions, was measured for each of the three scenarios. Lastly, heatmap visualizations of von Mises stress, which summarizes the distribution of forces on a structure under load, were generated from one model for each of the extant genera, and for all fossil specimens modeled.

**Statistical Analyses.** We evaluated data support for our stated hypotheses using analysis of variance (ANOVA). The tooth macrowear categories were used as groups, and ANOVA tests were conducted separately for the canine and carnassial macrowear of bone cracking

hypercarnivores (*Crocota crocuta*), scavenging hypercarnivores (*Hyaena hyaena* and *Parahyaena brunnea*), meat specialist hypercarnivores (*Panthera leo* and *Acinonyx jubatus*), and the fossil genus *Hyaenodon*. Morphofunctional traits evaluated against macrowear categories included input muscle force (in Newtons), output bite point reaction force (in Newtons), mechanical efficiency (output bite point reaction force/input muscle force), strain energy (J), total model volume (mm<sup>3</sup>), jaw length (mm), and jaw width (mm). Additionally, results were visualized as boxplots using R programming packages *ggplot2* and *ggpubr* (Wickham, 2016). All statistical tests were conducted in R using the *aov* function in the core R library.

## Results

**Tooth macrowear analysis.** All but one meat specialist carnassial examined (20 out of 21) exhibited little to no macrowear. By contrast, all three categories of macrowear are recorded for the canine position of meat specialists (Table S1). The majority of canine and carnassial macrowear scores are 2 or 3 in the scavenger data partition, and in bone crackers about half of the specimens have macrowear scores of 2 or 3. The majority of *Hyaenodon* specimens have a macrowear category of 2 or 3 in both canine and carnassial tooth positions.

**Jaw measurements.** Meat specialists in our dataset have a mean jaw length of 167.06 mm, mean jaw depth at canine of 31.60 mm, and mean jaw depth at m1 of 31.46 mm. Scavengers have a mean jaw length of 165.24 mm, canine jaw depth of 32.58 mm, and m1 jaw depth of 37.72 mm. Bone crackers have a mean jaw length of 162.97 mm, canine jaw depth of 29.88 mm, and carnassial jaw depth of 39.13 mm. Lastly, the *Hyaenodon* specimens studied have a mean jaw length of 179.78 mm, canine jaw depth of 24.96 mm, and carnassial jaw depth of 35.40 mm.

Based on these measurements, meat specialists have a nearly 1:1 ratio of jaw depth at the carnassial versus the canine, scavengers have 16% deeper mandibular ramus at the carnassial compared to the canine position, and bone crackers have ~30% deeper ramus at the carnassial compared to the canine position. In this regard, *Hyaenodon* is closest to bone crackers in having 41.6% deeper jaws at the carnassial compared to the canine position.

No clear patterns of jaw measurement differences across macrowear categories are present for either the canine or carnassial data of all ecomorph partitions (Fig. 2). Furthermore, none of the ANOVA tests returned statistically significant results (p values range from 0.90 to 0.06; Table 2).

**Biomechanical performance estimates.** Bone crackers at later macrowear stages tend to possess larger muscle insertion areas and therefore larger muscle input forces than other feeding ecologies, even though they are not overall the largest individuals in the dataset (Fig. 3). Canine bite mechanical efficiency values do not exhibit clear trends across macrowear categories in any feeding ecologies; however, bone crackers show increasing carnassial bite mechanical efficiency with increasing macrowear (Fig. 3D, Table 2;  $F = 9.31$ ,  $p = 0.02$ ). *Hyaenodon* exhibit increasing canine mechanical efficiency ( $F = 8.95$ ,  $p = 0.03$ ; Table 2) but no change in carnassial mechanical efficiency with increasing macrowear.

Meat specialists tend to exhibit increased strain energy (lower work efficiency or stiffness) at macrowear category 3 compared to other categories in canine biting (Fig. 4A-B), and a larger spread of strain energy values at macrowear category 1 in carnassial bite simulations (Fig. 4C).



None of the strain energy patterns are statistically significant (Table 2). In m1 bite reaction force, bone crackers alone exhibit a significant increase with increasing macrowear ( $F = 6.32$ ,  $p = 0.04$ ; Table 2, Fig. 4D), mirroring the pattern observed in m1 mechanical efficiency (Fig. 3D).

Heatmap visualization of von Mises stress in exemplary jaw models shows qualitatively that meat specialists tend to experience higher stresses than other feeding ecologies. In all canine bite simulations, the largest region of elevated stress is in the transition between the horizontal and ascending rami, immediately posterior to the carnassial (Fig. 5A-E). Bone crackers exhibit the lowest stress in the core of the horizontal ramus compared to other ecomorphs, displaying parallel strips of elevated stress at the dorsal and ventral edges of the mandible, respectively. All *Hyaenodon* specimens studied show a similar strip of low stress region along the length of the horizontal ramus in patterns most similar to bone crackers (Fig. 5F-N). In canine pull simulations the overall von Mises stress distributions are similar to those observed in canine bite simulations. The major difference is a relatively more stressed venter border along the horizontal ramus when a canine bite is combined with an anterior pulling force (Fig. 6).

The carnassial bite simulations differ from canine simulations in having more limited regions of high stress (Fig. 7). Meat specialists and scavengers tend to exhibit a continuous path of elevated stress connecting the dorsal and ventral horizontal stress paths ventral to the carnassial bite position. The bone cracking *Crocota* and the morphologically robust scavenger *Parahyaena* show the least amount of elevated stress along that dorsoventral path. Similarly, the von Mises stress patterns for carnassial biting in *Hyaenodon* specimens tend to show two separate elevated stress paths at the dorsal and ventral margins of the ramus, respectively. As expected, the

unloaded region of the mandible anterior to the bite point does not show elevated von Mises stress in any of the models visualized.

## Discussion

Bite simulation and macrowear analyses of hypercarnivore mandible models show that for meat specialists and scavengers there is no evidence of morphofunctional compensation in mandibular performance with increased tooth wear. However, there is a statistically significant increase in carnassial bite mechanical efficiency with increasing macrowear in bone cracking hypercarnivores. There is no correlation between macrowear and either jaw strain energy (a measure of work efficiency or stiffness) or jaw dimensional changes in any of the feeding ecologies studied. These results provide only partial support for our first hypothesis ( $H_1$ ), that bone crackers and scavengers exhibit morphofunctional compensation in mandible performance with increasing tooth macrowear whereas meat specialists do not.

The extinct carnivore *Hyaenodon* shared no statistically significant wear-dependent morphofunctional shifts with any of the extant feeding ecologies. Instead, the fossil taxon exhibits increased canine bite mechanical efficiency with increased tooth macrowear, differing from the bone crackers which show carnassial mechanical efficiency increase with macrowear. These findings provide no biomechanical support for the prior interpretation of *Hyaenodon* (as the name also suggests) as ecological equivalents of hyaenids in their respective paleoguilds. Therefore, we reject our second hypothesis ( $H_2$ ), that *Hyaenodon* and extant bone cracking and scavenging hyaenids share similar patterns of morphofunctional compensation with increasing tooth macrowear.

315

316 Previous studies on the functional morphology of *Hyaenodon* suggest a semi-arboreal locomotor  
 317 ecology for *H. exiguus* (Pfaff et al., 2017), with comparable or more specialized dental crown  
 318 features than the most specialized feliforms (Lang, Engler & Martin, 2022), reduced zygomatic  
 319 arch robustness associated with capability for higher gape (De Iuliis, 1993), and similarity to  
 320 hyenas or lions in dental microwear depending on geographic region (Bastl, Semprebon &  
 321 Nagel, 2012). What emerges from these studies and new findings reported in the current study  
 322 is that (1) there is no single living ecomorphology that converges on *Hyaenodon* in terms of the  
 323 morphofunctional traits analyzed, and (2) there is diversity in the range of dietary ecologies  
 324 within the genus *Hyaenodon*. Therefore, the lack of a match in the morphofunctional traits  
 325 measured in this study between *Hyaenodon* and extant hypercarnivore feeding ecologies may  
 326 reflect a combination of unique niches occupied by *Hyaenodon* and a possible mixture of  
 327 ecomorphs represented in our *Hyaenodon* dataset. We combined different species of *Hyaenodon*  
 328 into a single dataset because of the small fossil sample sizes available; this may have reduced the  
 329 functional morphological signal available in the data by mixing multiple ecomorphs. Future  
 330 research that focuses on larger single-taxon samples of *Hyaenodon* will permit a test of this  
 331 interpretation.

332

333 The absence of morphofunctional correlates of tooth macrowear in the meat specialist and  
 334 scavenging hypercarnivore species studied indicates that either (1) tooth wear has no significant  
 335 impact on biting performance, or (2) tooth wear does influence biting performance but there is no  
 336 morphofunctional compensation. In the case of meat specialists, it may be that advanced tooth  
 337 macrowear is rarer than in other ecomorphs with more mechanically demanding diets (Table S1),

rendering morphofunctional compensation unnecessary or too subtle to be detected with the current dataset. In some extant puma populations, both age-dependent and life stage-dependent differences in predation patterns have been observed (Elbroch, Feltner & Quigley, 2017; Elbroch & Quigley, 2019). Dispersing pumas tend to go after smaller prey, whereas older pumas tend to take down larger prey. Both observations suggest that behavioral shifts play a role in predation and constitute another dimension of compensation for individual condition and age (which includes tooth wear) beyond morphofunctional traits. The presence of other predators, including the relative abundance of co-occurring wolves in North America, can also mediate dietary choices including the size and condition of prey species in pumas (Kortello et al. 2007; Bartnick et al. 2013) – with pumas consuming prey with the greatest range of body sizes as compared to neotropical carnivores (Cruz et al., 2022). On the other hand, no significant dietary differences were observed among individuals of a high-density jaguar (*Panthera onca*) population (Foster & Harmsen, 2022). Thus, there may be a large range of behavioral plasticity that masks any morphofunctional response to decreased masticatory capability with increased tooth macrowear, at least in meat specialists.

In the bone cracking spotted hyenas (*Crocuta crocuta*), there is a range of hunting group sizes that correlates with individual age. Older spotted hyenas tend to hunt alone more frequently than younger individuals (Holekamp et al., 1997). In contrast, the scavengers brown hyenas (*Parahyaena brunnea*) and striped hyenas (*Hyaena hyaena*) tend to hunt and scavenge solo regardless of age, and instead scavenge in larger groups where all individuals access a similar food source (Owens & Owens, 1978; Watts & Holekamp, 2007). Our findings are consistent with these observed behavioral differences. Bone crackers exhibit significantly increased

carnassial bite mechanical efficiency with tooth macrowear typical of older individuals who hunt alone more frequently. Scavengers show a non-significant increase in mechanical efficiency from the lowest macrowear category to the higher categories (Fig. 3D), and correspondingly do not show age-related differences in hunting strategy. Furthermore, the absence of wear-dependent morphofunctional changes in other measured traits (jaw dimensions, canine and carnassial bite strain energy, canine bite mechanical efficiency) in bone crackers may be in part explained by social rank structured feeding behavior in that species; higher ranked individuals have preferential access to food resources regardless of whether those same individuals were responsible for the acquisition of a particular meal (Kruuk, 1972). Priority access to softer parts of a prey carcass by virtue of high social rank would permit some individuals to obtain high quality food even if their masticatory system performs suboptimally for mechanically demanding tasks because of tooth wear and damage.

One strength of our 2D based approach to estimating biomechanical performance is the ability to incorporate larger sample sizes in our finite element modeling compared to most previous studies of similar scope. The current paradigm of using FEA to correlate organismal form and function often relies on only one or two specimen models per species because of the time-consuming nature of FE protocols (Tseng, 2021). As such, no previous studies have examined individual differences in the biomechanical traits analyzed herein as a consequence of tooth wear and tear.

On the other hand, the 2D modeling approach limits our examination of biomechanical performance to the dorsoventral plane. The origin of mammalian mastication/chewing has been speculated to involve pitch and yaw components that provide more nuanced movements of the

hemimandibles and thus angles of occlusion (Bhullar et al., 2019). Although the plane of wear on the carnassial teeth of carnivorans and hyaenodontids are largely in the dorsoventral direction, indicating the principal movement of occlusion to be dorsoventrally oriented, there may be important shear forces on the masticatory system that results in this study could not account for. Future studies of form-function linkage in a tooth macrowear context would benefit from a critical analysis of the extent that 3D information is consistent with, or adds substantially to, the 2D biomechanical data collected in the present study.

## Conclusions

In this study we hypothesized that bone cracking and scavenging hypercarnivores should exhibit morphofunctional compensation with more severe tooth macrowear, whereas meat specialists do not have the mechanical need to make such adjustments. We found only partial support for this prediction, with results showing that the carnassial bite mechanical efficiency of bone cracking ecomorphs is the only performance attribute that is significantly correlated with the extent of tooth macrowear. We further hypothesized that the extinct carnivore *Hyaenodon*, commonly thought to be functionally convergent with extant hyaenids, would share similar patterns of morphofunctional compensation with tooth wear. We found that *Hyaenodon* is unique among the hypercarnivores studied in exhibiting canine bite mechanical efficiency increase with tooth macrowear, an observation that rejects our second hypothesis. The incorporation of tooth macrowear patterns into assessments of morphofunctional traits provides an explicit link between form-function linkages at the interspecific level, and tooth wear and age at the individual level. These findings support the inference that rather than treating feeding ecologies as static and characterizable by single specimen models, the morphofunctional trajectories of

tooth use, tooth wear, and jaw mechanics can provide an added dimension of biomechanical performance profiling for a given taxon. These observations highlight the mammalian masticatory system as having a dynamic performance profile through its useful lifespan, and encourage a more nuanced understanding of past and present carnivore guilds by considering wear-dependent performance changes as a possible source of selection.

## Acknowledgements

We acknowledge N. Lo and L. Chen for their assistance with image curation and model preparation. E. Westwig (formerly of AMNH) assisted with access to the AMNH Mammalogy collections. J. Flynn and R. O’Leary assisted with access to the AMNH Paleontology collections. ZJT thanks J. Liu for discussion during the initial stages of manuscript writing.

# References

- Bartnick TD, Van Deelen TR, Quigley HB, and Craighead D. 2013. Variation in cougar (*Puma concolor*) predation habits during wolf (*Canis lupus*) recovery in the southern Greater Yellowstone Ecosystem. *Canadian Journal of Zoology*. 91(2): 82-93.  
<https://doi.org/10.1139/cjz-2012-0147>
- Bastl K, Semprebon G, Nagel D. 2012. Low-magnification microwear in Carnivora and dietary diversity in Hyaenodon (Mammalia: Hyaenodontidae) with additional information on its enamel microstructure. *Palaeogeography, Palaeoclimatology, Palaeoecology* 348–349:13–20. DOI: <https://doi.org/10.1016/j.palaeo.2012.05.026>.
- Bhullar B-AS, Manafzadeh AR, Miyamae JA, Hoffman EA, Brainerd EL, Musinsky C, Crompton AW. 2019. Rolling of the jaw is essential for mammalian chewing and tribosphenic molar function. *Nature* 566:528–532. DOI: 10.1038/s41586-019-0940-x.
- Bourke J, Wroe S, Moreno K, McHenry C, Clausen P. 2008. Effects of gape and tooth position on bite force and skull stress in the dingo (*Canis lupus dingo*) using a 3-dimensional finite element approach. *PLoS one* 3:e2200.
- Burt AA, DeSantis LRG. 2022. Exploring durophagy among modern gray wolves from the Greater Yellowstone Ecosystem with dental microwear texture analysis. *Journal of Zoology* 317:22–33.
- Cruz, LR, Muylaert, RL, Galetti, M, Pires, MM. 2022. The geography of diet variation in Neotropical Carnivora. *Mammal Review*, 52(1):112–128. DOI: 10.1111/mam.12266
- DeSantis LRG. 2016. Dental microwear textures: reconstructing diets of fossil mammals. *Surface Topography: Metrology and Properties* 4:23002. DOI: 10.1088/2051-672x/4/2/023002.



443 DeSantis LRG, Schubert BW, Schmitt-Linville E, Ungar PS, Donohue SL, Haupt RJ. 2015.  
444 Dental Microwear Textures of Carnivorans from the La Brea Tar Pits, California, and  
445 Potential Extinction Implications. *Natural History Museum of Los Angeles County Science*  
446 *Series* 42:37–52.

447 DeSantis LRG, Tseng ZJ, Liu J, Hurst A, Schubert BW, Jiangzuo Q. 2017. Assessing niche  
448 conservatism using a multiproxy approach: dietary ecology of extinct and extant spotted  
449 hyenas. *Paleobiology* 43:286–303. DOI: DOI: 10.1017/pab.2016.45.

450 Elbroch LM, Feltner J, Quigley HB. 2017. Stage-dependent puma predation on dangerous prey.  
451 *Journal of Zoology* 302:164–170. DOI: <https://doi.org/10.1111/jzo.12442>.

452 Elbroch LM, Quigley H. 2019. Age-specific foraging strategies among pumas, and its  
453 implications for aiding ungulate populations through carnivore control. *Conservation*  
454 *Science and Practice* 1:e23. DOI: <https://doi.org/10.1111/csp2.23>.

455 Evans HE, Christensen GC (eds.). 1979. *Miller's anatomy of the dog*. Philadelphia: Saunders, an  
456 imprint of Elsevier, Inc.

457 Foster RJ, Harmsen BJ. 2022. Dietary similarity among jaguars (*Panthera onca*) in a high-density  
458 population. *PLOS ONE* 17:e0274891.

459 Goldstein JI, Newbury DE, Michael JR, Ritchie NWM, Scott JHJ, Joy DC, Goldstein JI,  
460 Newbury DE, Michael JR, Ritchie NWM. 2018. ImageJ and Fiji. *Scanning electron*  
461 *microscopy and X-ray microanalysis*:187–193.

462 Grosse IR, Dumont ER, Coletta C, Tolleson A. 2007. Techniques for Modeling Muscle-induced  
463 Forces in Finite Element Models of Skeletal Structures. *The Anatomical Record* 290:1069–  
464 1088. DOI: <https://doi.org/10.1002/ar.20568>.

465 Holekamp KE, Smale L, Berg R, Cooper SM. 1997. Hunting rates and hunting success in the

466 spotted hyena (*Crocuta crocuta*). *Journal of Zoology* 242:1–15. DOI:  
 467 <https://doi.org/10.1111/j.1469-7998.1997.tb02925.x>.

468 De Iuliis G. 1993. The Zygomatic Arch of Hyaenodon (Hyaenodontidae: Creodonta). *Journal of*  
 469 *Mammalogy* 74:347–351. DOI: 10.2307/1382390.

470 Jones KE, Bielby J, Cardillo M, Fritz SA, O’Dell J, Orme CDL, Safi K, Sechrest W, Boakes EH,  
 471 Carbone C, Connolly C, Cutts MJ, Foster JK, Grenyer R, Habib M, Plaster CA, Price SA,  
 472 Rigby EA, Rist J, Teacher A, Bininda-Emonds ORP, Gittleman JL, Mace GM, Purvis A.  
 473 2009. PanTHERIA: a species-level database of life history, ecology, and geography of  
 474 extant and recently extinct mammals. *Ecology* 90:2648. DOI: [https://doi.org/10.1890/08-](https://doi.org/10.1890/08-1494.1)  
 475 1494.1.

476 Kortello AD, Hurd TD, and Murray DL. 2007. Interactions between cougars (*Puma concolor*)  
 477 and gray wolves (*Canis lupus*) in Banff National Park, Alberta. *Ecoscience* 14(2):214-222.

478 Kruuk H. 1972. *The Spotted Hyena*. Chicago: University of Chicago Press.

479 Lang AJ, Engler T, Martin T. 2022. Dental topographic and three-dimensional geometric  
 480 morphometric analysis of carnassialization in different clades of carnivorous mammals  
 481 (Dasyuromorphia, Carnivora, Hyaenodonta). *Journal of Morphology* 283:91–108.

482 Lucas PW, van Casteren A. 2014. The Wear and Tear of Teeth. *Medical Principles and Practice*  
 483 24:3–13. DOI: 10.1159/000367976.

484 Luo Z-X, Kielan-Jaworoska Z, Cifelli RL. 2004. Evolution of dental replacement in mammals.  
 485 *Bulletin of Carnegie Museum of Natural History*:159–175. DOI: 10.2992/0145-  
 486 9058(2004)36[159:EODRIM]2.0.CO;2.

487 Owens MJ, Owens DD. 1978. Feeding ecology and its influence on social organization in brown  
 488 hyenas (*Hyaena brunnea*, Thunberg) of the central Kalahari Desert. *African Journal of*

489       *Ecology* 16:113–135.

490 Pfaff C, Nagel D, Gunnell G, Weber GW, Kriwet J, Morlo M, Bastl K. 2017. Palaeobiology of

491       Hyaenodon exiguus (Hyaenodonta, Mammalia) based on morphometric analysis of the

492       bony labyrinth. *Journal of Anatomy* 230:282–289. DOI: <https://doi.org/10.1111/joa.12545>.

493 Tseng ZJ. 2021. Rethinking the use of finite element simulations in comparative biomechanics

494       research. *PeerJ* 9:e11178. DOI: [10.7717/peerj.11178](https://doi.org/10.7717/peerj.11178).

495 Tseng ZJ, Binder WJ. 2010. Mandibular biomechanics of *Crocota crocuta*, *Canis lupus*, and the

496       late Miocene *Dinocrocota gigantea* (Carnivora, Mammalia). *Zoological Journal of the*

497       *Linnean Society* 158:683–696.

498 Tseng ZJ, Garcia-Lara S, Flynn JJ, Holmes E, Rowe TB, Dickson B V. 2023. A switch in jaw

499       form–function coupling during the evolution of mammals. *Philosophical Transactions of*

500       *the Royal Society B: Biological Sciences* 378:20220091. DOI: [10.1098/rstb.2022.0091](https://doi.org/10.1098/rstb.2022.0091).

501 Tseng ZJ, Stynder D. 2011. Mosaic functionality in a transitional ecomorphology: skull

502       biomechanics in stem Hyaeninae compared to modern South African carnivorans.

503       *Biological Journal of the Linnean Society* 102:540–559. DOI: [10.1111/j.1095-](https://doi.org/10.1111/j.1095-8312.2010.01602.x)

504       8312.2010.01602.x.

505 Van Valkenburgh B. 2007. Déjà vu: the evolution of feeding morphologies in the Carnivora.

506       *Integrative and Comparative Biology* 47:147–163. DOI: [10.1093/icb/icm016](https://doi.org/10.1093/icb/icm016).

507 Watts HE, Holekamp KE. 2007. Hyena societies. *Current Biology* 17:R657–R660. DOI:

508       [10.1016/j.cub.2007.06.002](https://doi.org/10.1016/j.cub.2007.06.002).

509 Werdelin L, Gittleman JL. 1996. Carnivoran ecomorphology: a phylogenetic perspective.

510       *Carnivore behavior, ecology, and evolution* 2:582–624.

511 Wickham H. 2016. *ggplot2: Elegant Graphics for Data Analysis*. New York: Springer-Verlag.

512 Wroe S, McHenry C, Thomason J. 2005. Bite club: comparative bite force in big biting  
 513 mammals and the prediction of predatory behaviour in fossil taxa. *Proceedings of the Royal*  
 514 *Society B: Biological Sciences* 272:619–625. DOI: 10.1098/rspb.2004.2986.  
 515  
 516

# Table and Figure Captions

**Table 1.** Sample size and feeding ecology assignments of taxa examined in this study.

**Table 2.** Results of ANOVA tests of morphofunctional traits across tooth macrowear categories by feeding ecology. P values < 0.05 are indicated in bold font.

**Figure 1.** Examples of bite simulation models for each of the four feeding ecologies and the fossil taxon studied. **A.** *Acinonyx jubatus*, a meat specialist; **B.** *Hyaena hyaena*, a scavenger; **C.** *Panthera leo*, a meat specialist; **D.** *Parahyaena brunnea*, a scavenger; **E.** *Crocota crocuta*, a bone cracker; **F.** *Hyaenodon crucians*, a fossil carnivore. Green silhouettes represent cranial reference shapes. Muscle insertion areas: temporalis (red), zygomaticomandibularis/deep masseter (blue), masseter/superficial masseter (orange). Centroid points for guiding muscle vector orientations are shown in the same colors as their respective muscle groups. Abbreviations: M, masseter; Mc, masseter centroid; T, temporalis; Tc, temporalis centroid; ZM, zygomaticomandibularis ; ZMc ; zygomaticomandibularis centroid.

**Figure 2.** Boxplots of morphofunctional trait values by macrowear category. **A.** Canine macrowear versus jaw model volume. **B.** Carnassial macrowear versus jaw model volume. **C.** Canine macrowear versus jaw length. **D.** Carnassial macrowear versus jaw length. **E.** Canine macrowear versus jaw depth at post-canine position. **F.** Carnassial macrowear versus jaw depth at post-carnassial position.

**Figure 3.** Boxplots of morphofunctional trait values by macrowear category. **A.** Canine macrowear versus input muscle force. **B.** Carnassial (m1) macrowear versus input muscle force. **C.** Canine macrowear versus canine bite mechanical efficiency. **D.** Carnassial macrowear versus carnassial bite mechanical efficiency.

**Figure 4.** Boxplots of morphofunctional trait values by macrowear category. **A.** Canine macrowear versus canine bite strain energy. **B.** Canine macrowear versus canine pull strain energy. **C.** Carnassial (m1) macrowear versus m1 bite strain energy. **D.** Carnassial macrowear versus m1 output bite point reaction force.

**Figure 5.** Heatmap visualization of von Mises stress from canine bite simulations. **A.** *Acinonyx jubatus*, AMNH-VP (extant element collection of AMNH Department of Vertebrate Paleontology) 2502; **B.** *Panthera leo*, UMMZ 114804; **C.** *Crocota crocuta*, UMMZ 114799; **D.** *Hyaena hyaena*, AMNH-VP 1544; **E.** *Parahyaena brunnea*, UMMZ 95748; **F.** *Hyaenodon brevirostris*, F:AM (Frick collection of the AMNH) 75629; **G.** *H. crucians*, F:AM 75596; **H.** *H. cruentus*, F:AM 75607; **I.** *H. cruentus*, F:AM 75692; **J.** *H. cruentus*, F:AM 75729; **K.** *H. exiguus*, AMNH 55314; **L.** *H. horridus*, F:AM 75704; **M.** *H. luskensis*, F:AM 75606; **N.** *H. paucidens*, AMNH 647.

**Figure 6.** Heatmap visualization of von Mises stress from canine pull simulations. **A.** *Acinonyx jubatus*, AMNH-VP (extant element collection of AMNH Department of Vertebrate Paleontology) 2502; **B.** *Panthera leo*, UMMZ 114804; **C.** *Crocota crocuta*, UMMZ 114799; **D.** *Hyaena hyaena*, AMNH-VP 1544; **E.** *Parahyaena brunnea*, UMMZ 95748; **F.** *Hyaenodon*

563 *brevirostris*, F:AM (Frick collection of the AMNH) 75629; **G.** *H. crucians*, F:AM 75596; **H.** *H.*  
 564 *cruentus*, F:AM 75607; **I.** *H. cruentus*, F:AM 75692; **J.** *H. cruentus*, F:AM 75729; **K.** *H.*  
 565 *exiguus*, AMNH 55314; **L.** *H. horridus*, F:AM 75704; **M.** *H. luskensis*, F:AM 75606; **N.** *H.*  
 566 *paucidens*, AMNH 647.

567

568 **Figure 7.** Heatmap visualization of von Mises stress from carnassial bite simulations. **A.**

569 *Acinonyx jubatis*, AMNH-VP (extant element collection of AMNH Department of Vertebrate  
 570 Paleontology) 2502; **B.** *Panthera leo*, UMMZ 114804; **C.** *Crocota crocuta*, UMMZ 114799; **D.**  
 571 *Hyaena hyaena*, AMNH-VP 1544; **E.** *Parahyaena brunnea*, UMMZ 95748; **F.** *Hyaenodon*  
 572 *brevirostris*, F:AM (Frick collection of the AMNH) 75629; **G.** *H. crucians*, F:AM 75596; **H.** *H.*  
 573 *cruentus*, F:AM 75607; **I.** *H. cruentus*, F:AM 75692; **J.** *H. cruentus*, F:AM 75729; **K.** *H.*  
 574 *exiguus*, AMNH 55314; **L.** *H. horridus*, F:AM 75704; **M.** *H. luskensis*, F:AM 75606; **N.** *H.*  
 575 *paucidens*, AMNH 647.

# Figure 1

Examples of bite simulation models for each of the four feeding ecologies and the fossil taxon studied.

**A.** *Acinonyx jubatus*, a meat specialist; **B.** *Hyaena hyaena*, a scavenger; **C.** *Panthera leo*, a meat specialist; **D.** *Parahyaena brunnea*, a scavenger; **E.** *Crocota crocuta*, a bone cracker; **F.** *Hyaenodon crucians*, a fossil carnivore. Green silhouettes represent cranial reference shapes. Muscle insertion areas: temporalis (red), zygomaticomandibularis/deep masseter (blue), masseter/superficial masseter (orange). Centroid points for guiding muscle vector orientations are shown in the same colors as their respective muscle groups. Abbreviations: M, masseter; Mc, masseter centroid; T, temporalis; Tc, temporalis centroid; ZM, zygomaticomandibularis; ZMc; zygomaticomandibularis centroid.

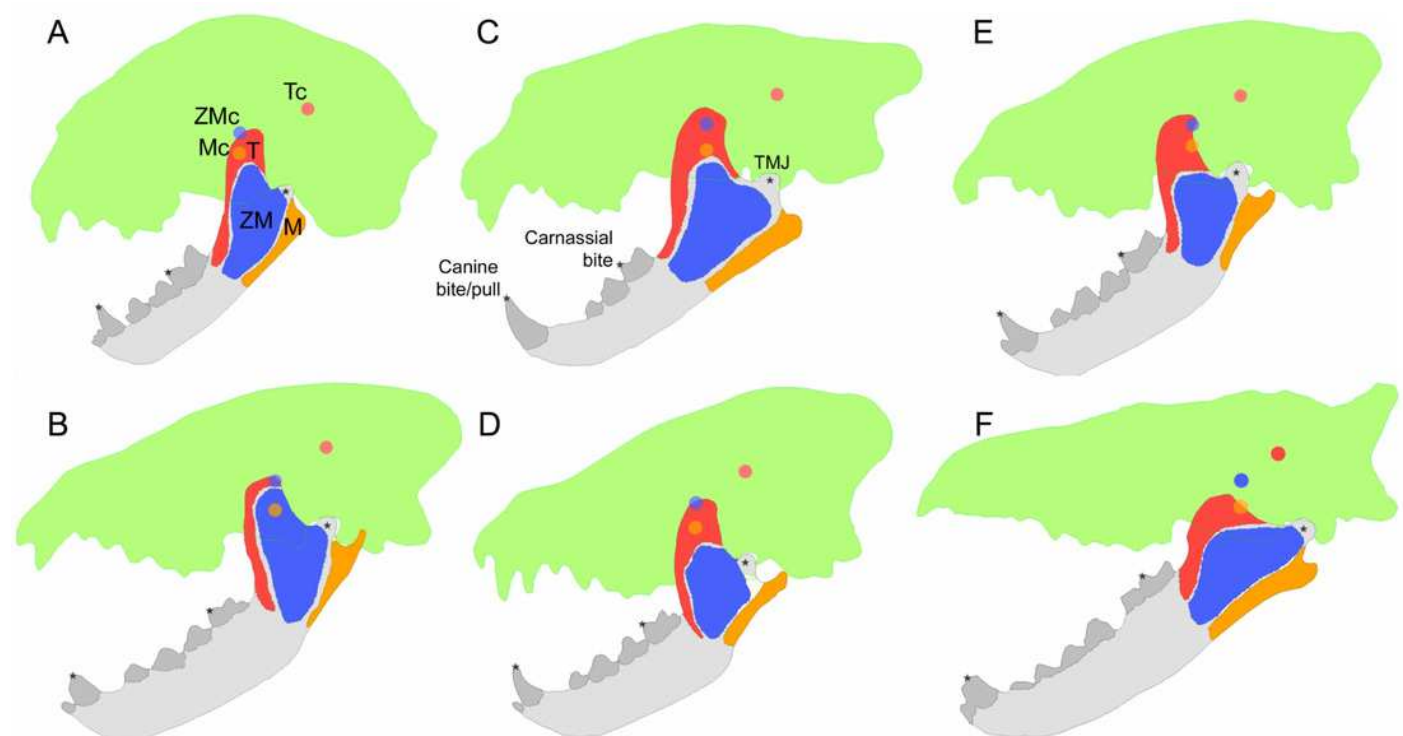




# Figure 2

Boxplots of morphofunctional trait values by macrowear category.

**A.** Canine macrowear versus jaw model volume. **B.** Carnassial macrowear versus jaw model volume. **C.** Canine macrowear versus jaw length. **D.** Carnassial macrowear versus jaw length. **E.** Canine macrowear versus jaw depth at post-canine position. **F.** Carnassial macrowear versus jaw depth at post-carnassial position.

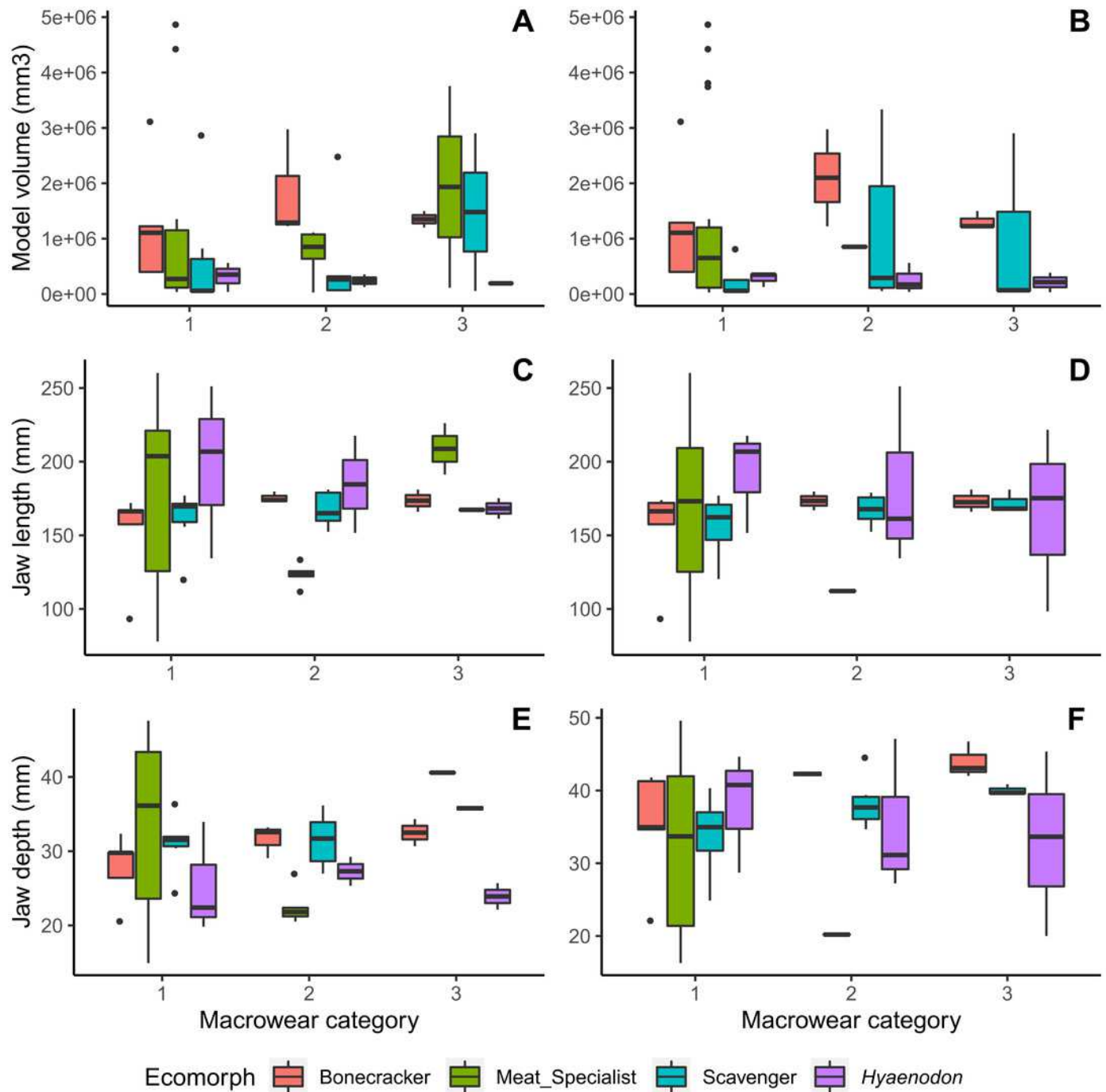


# Figure 3

Boxplots of morphofunctional trait values by macrowear category.

**A.** Canine macrowear versus input muscle force. **B.** Carnassial (m1) macrowear versus input muscle force. **C.** Canine macrowear versus canine bite mechanical efficiency. **D.** Carnassial macrowear versus carnassial bite mechanical efficiency.

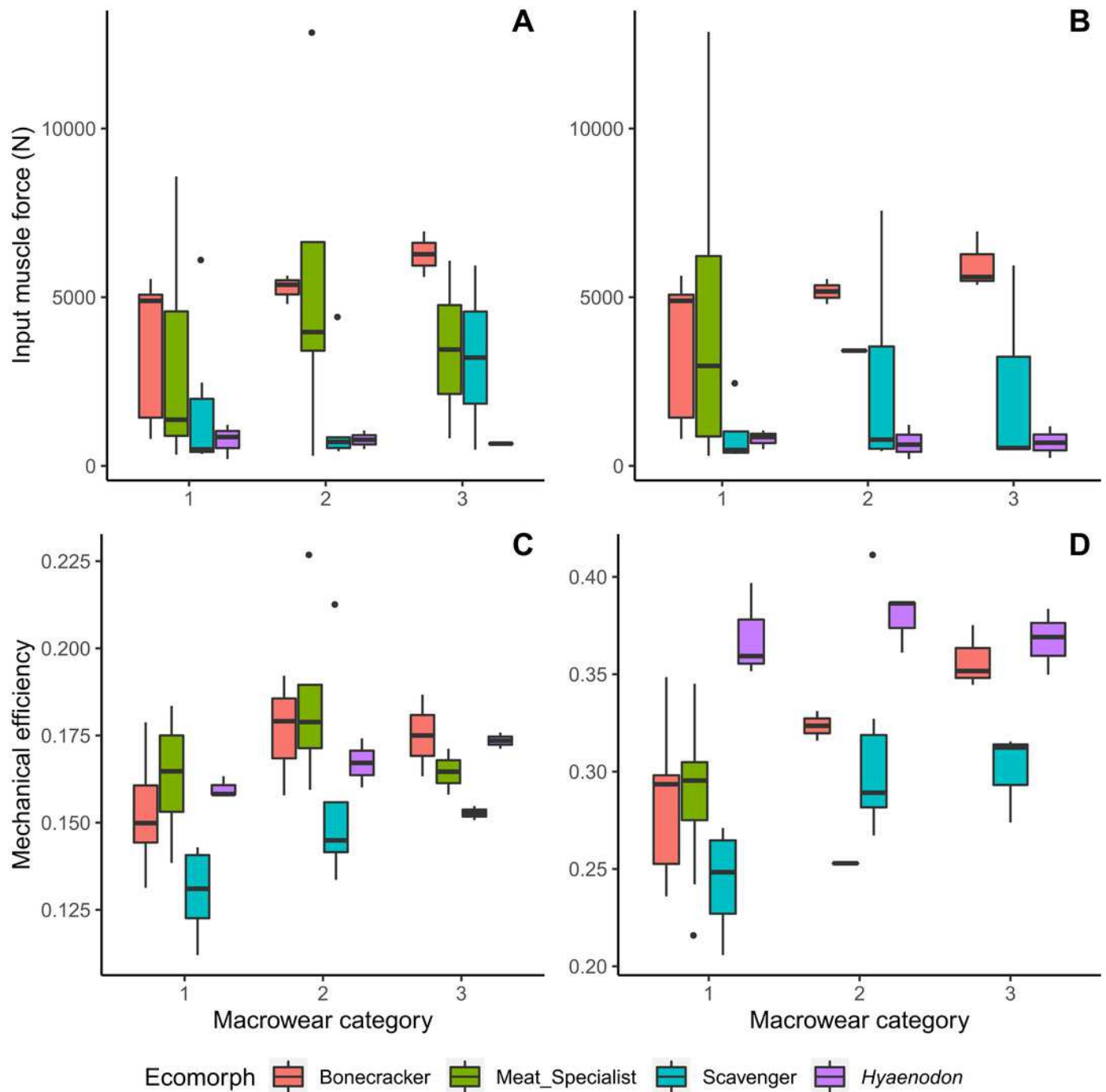


# Figure 4

Boxplots of morphofunctional trait values by macrowear category.

**A.** Canine macrowear versus canine bite strain energy. **B.** Canine macrowear versus canine pull strain energy. **C.** Carnassial (m1) macrowear versus m1 bite strain energy. **D.** Carnassial macrowear versus m1 output bite point reaction force.

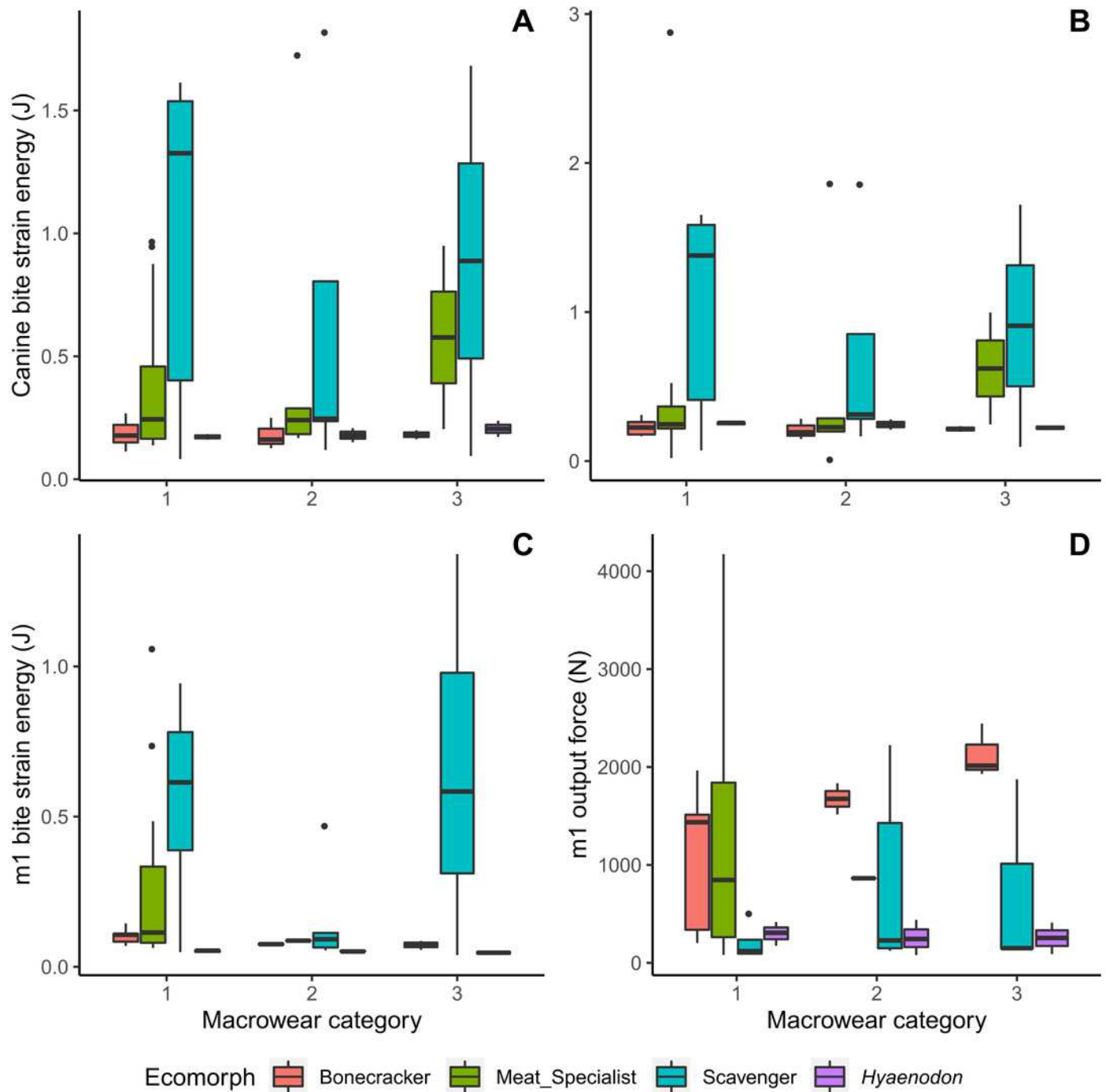


# Figure 5

Heatmap visualization of von Mises stress from canine bite simulations.

**A.** *Acinonyx jubatis*, AMNH-VP (extant element collection of AMNH Department of Vertebrate Paleontology) 2502; **B.** *Panthera leo*, UMMZ 114804; **C.** *Crocota crocuta*, UMMZ 114799; **D.** *Hyaena hyaena*, AMNH-VP 1544; **E.** *Parahyaena brunnea*, UMMZ 95748; **F.** *Hyaenodon brevirostris*, F:AM (Frick collection of the AMNH) 75629; **G.** *H. crucians*, F:AM 75596; **H.** *H. cruentus*, F:AM 75607; **I.** *H. cruentus*, F:AM 75692; **J.** *H. cruentus*, F:AM 75729; **K.** *H. exiguus*, AMNH 55314; **L.** *H. horridus*, F:AM 75704; **M.** *H. luskensis*, F:AM 75606; **N.** *H. paucidens*, AMNH 647.

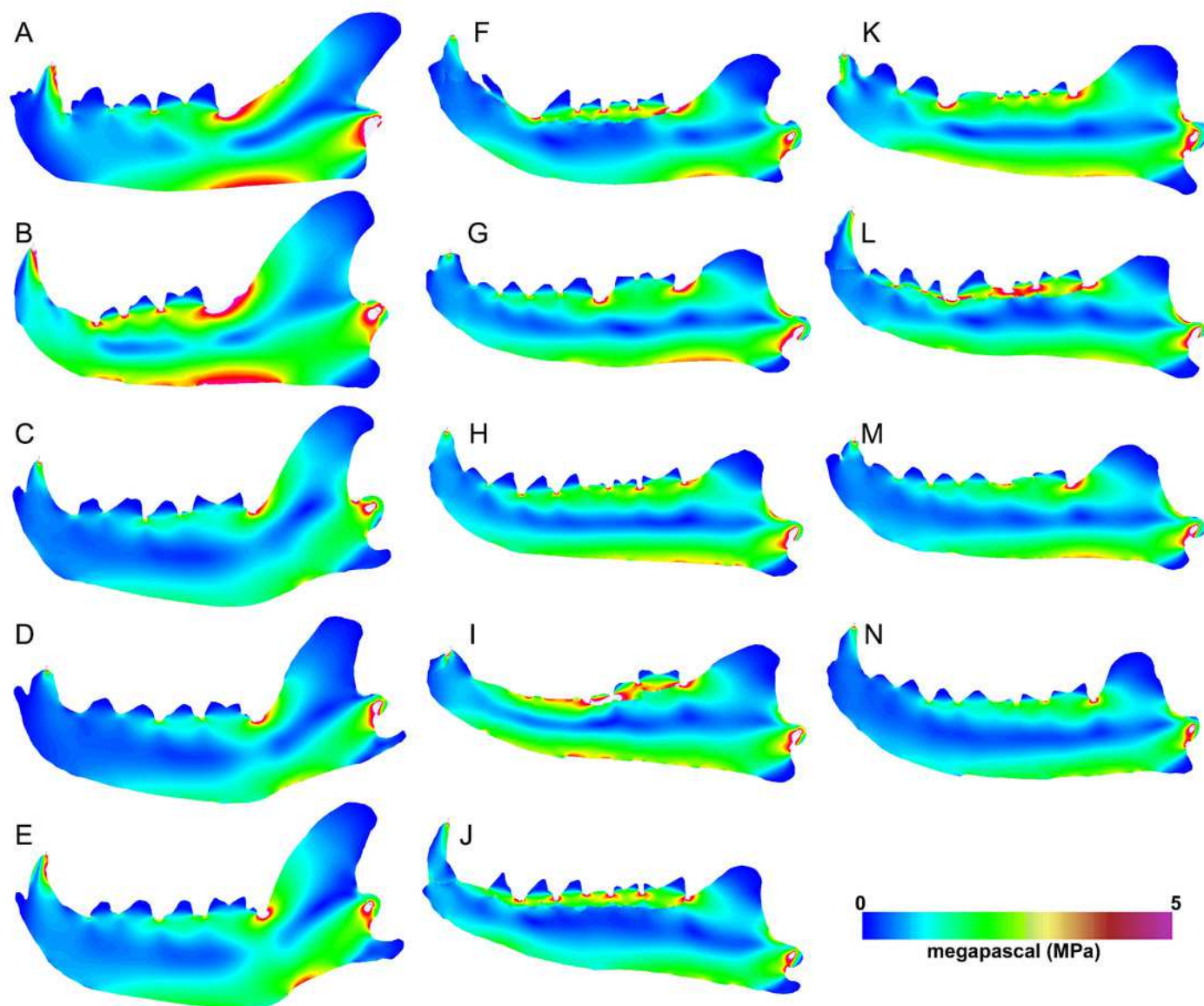




# Figure 6

Heatmap visualization of von Mises stress from canine pull simulations.

**A.** *Acinonyx jubatis*, AMNH-VP (extant element collection of AMNH Department of Vertebrate Paleontology) 2502; **B.** *Panthera leo*, UMMZ 114804; **C.** *Crocota crocuta*, UMMZ 114799; **D.** *Hyaena hyaena*, AMNH-VP 1544; **E.** *Parahyaena brunnea*, UMMZ 95748; **F.** *Hyaenodon brevirostris*, F:AM (Frick collection of the AMNH) 75629; **G.** *H. crucians*, F:AM 75596; **H.** *H. cruentus*, F:AM 75607; **I.** *H. cruentus*, F:AM 75692; **J.** *H. cruentus*, F:AM 75729; **K.** *H. exiguus*, AMNH 55314; **L.** *H. horridus*, F:AM 75704; **M.** *H. luskensis*, F:AM 75606; **N.** *H. paucidens*, AMNH 647.

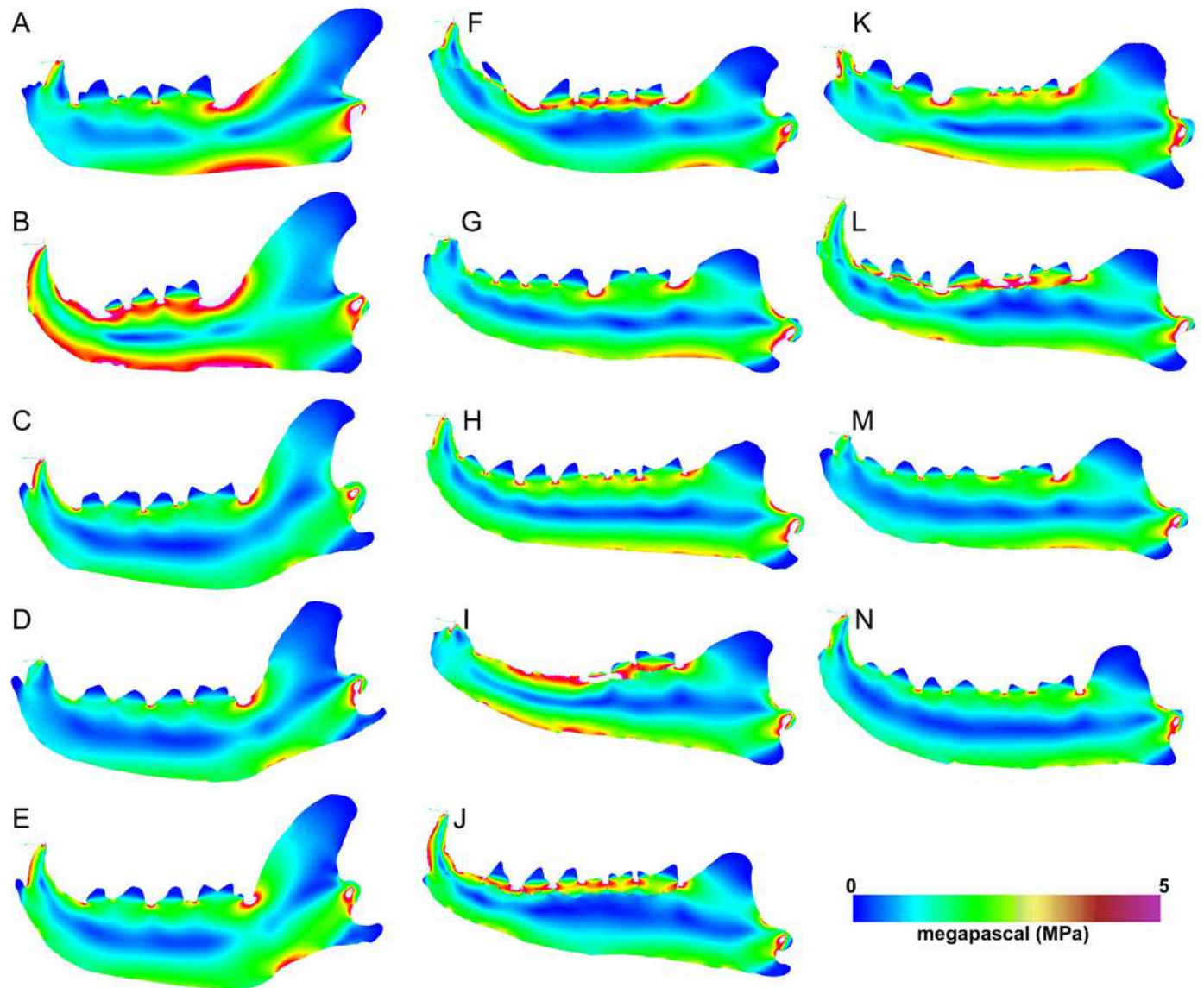


# Figure 7

Heatmap visualization of von Mises stress from carnassial bite simulations.

**A.** *Acinonyx jubatis*, AMNH-VP (extant element collection of AMNH Department of Vertebrate Paleontology) 2502; **B.** *Panthera leo*, UMMZ 114804; **C.** *Crocota crocuta*, UMMZ 114799; **D.** *Hyaena hyaena*, AMNH-VP 1544; **E.** *Parahyaena brunnea*, UMMZ 95748; **F.** *Hyaenodon brevirostris*, F:AM (Frick collection of the AMNH) 75629; **G.** *H. crucians*, F:AM 75596; **H.** *H. cruentus*, F:AM 75607; **I.** *H. cruentus*, F:AM 75692; **J.** *H. cruentus*, F:AM 75729; **K.** *H. exiguus*, AMNH 55314; **L.** *H. horridus*, F:AM 75704; **M.** *H. luskensis*, F:AM 75606; **N.** *H. paucidens*, AMNH 647.

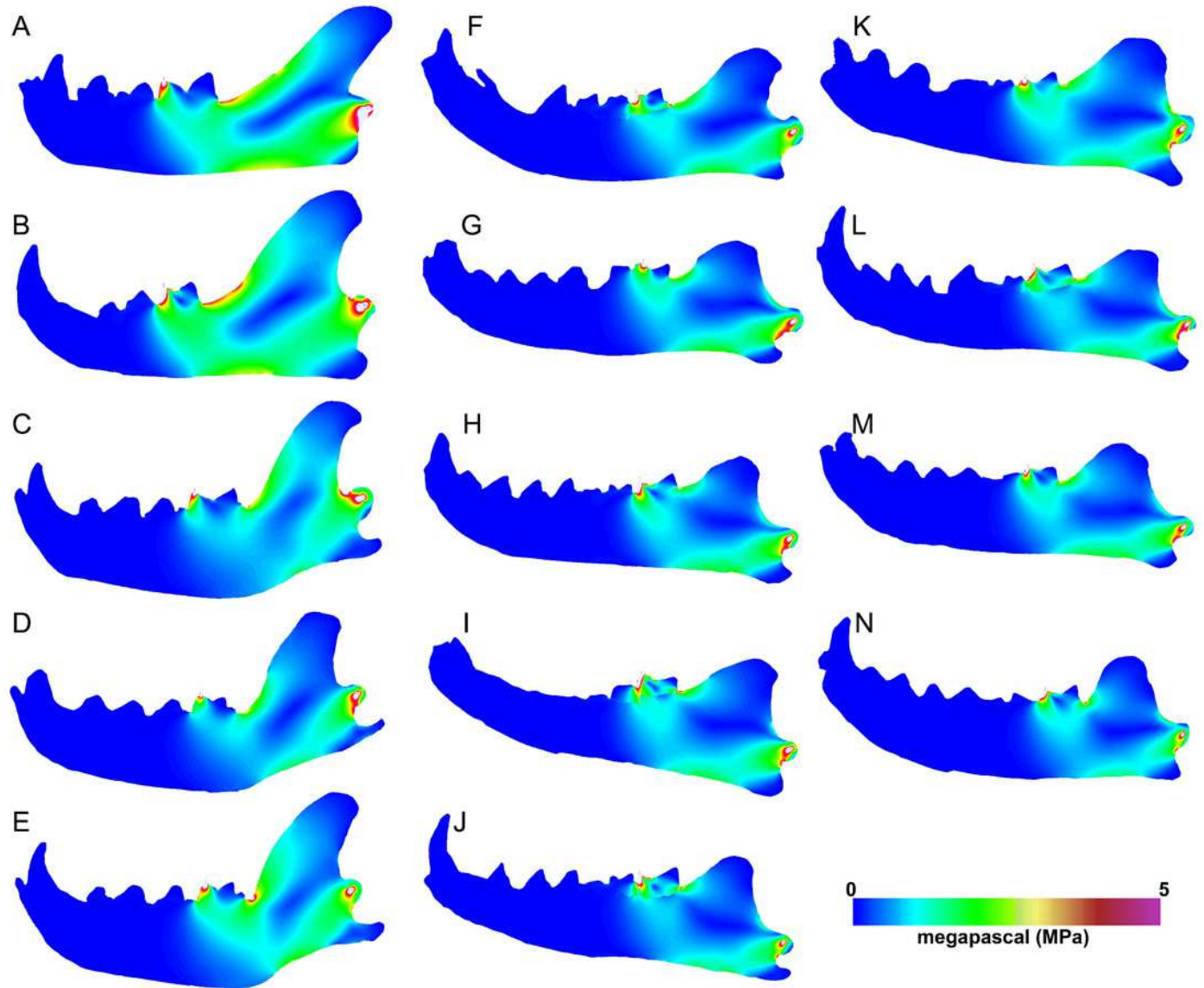


**Table 1** (on next page)

Sample size and feeding ecology assignments of taxa examined in this study.

Ecomorph	Genus	Species	Sample size
Bone cracker	<b><i>Crocuta</i></b>	<b><i>crocuta</i></b>	<b>10</b>
Meat specialist	<i>Acinonyx</i>	<i>jubatus</i>	10
	<i>Panthera</i>	<i>leo</i>	11
		<b>Meat specialist total</b>	<b>21</b>
Scavenger	<i>Hyaena</i>	<i>hyaena</i>	7
	<i>Parahyaena</i>	<i>brunnea</i>	7
		<b>Scavenger total</b>	<b>14</b>
Fossil	<i>Hyaenodon</i>	<i>paucidens</i>	1
	<i>Hyaenodon</i>	<i>exiguus</i>	1
	<i>Hyaenodon</i>	<i>crucians</i>	1
	<i>Hyaenodon</i>	<i>luskensis</i>	1
	<i>Hyaenodon</i>	<i>brevirostris</i>	1
	<i>Hyaenodon</i>	<i>horridus</i>	1
	<i>Hyaenodon</i>	<i>cruentus</i>	3
		<b>Fossil total</b>	<b>9</b>
		<b>All models total</b>	<b>54</b>

1

# **Table 2**(on next page)

Results of ANOVA tests of morphofunctional traits across tooth macrowear categories by feeding ecology.

P values < 0.05 are indicated in bold font.

Macrowear category	Morphofunctional trait	Bone cracker		Meat specialist		Scavenger		<i>Hyaenodon</i>	
		<i>F</i>	<i>p</i>	<i>F</i>	<i>p</i>	<i>F</i>	<i>p</i>	<i>F</i>	<i>p</i>
Canine macrowear	Input muscle force (N)	<u>4.52</u>	<u>0.07</u>	0.71	0.41	0.33	0.58	0.07	0.80
	Mechanical Efficiency	3.27	0.11	1.27	0.28	3.01	0.11	<b>8.95</b>	<b>0.03</b>
	Strain Energy (Bite; J)	0.02	0.90	0.48	0.50	0.20	0.66	1.43	0.29
	Strain Energy (Pull; J)	0.14	0.72	0.05	0.82	0.19	0.67	1.44	0.28
	Model Volume (mm <sup>3</sup> )	0.11	0.75	0.10	0.76	0.49	0.50	0.57	0.48
	Jaw length (mm)	1.75	0.22	0.05	0.83	0.44	0.52	0.55	0.49
	Jaw depth (mm)	3.14	0.11	0.02	0.90	1.94	0.19	0.06	0.81
Carnassial macrowear	Input muscle force (N)	4.04	0.08	0.01	0.92	0.61	0.45	0.10	0.77
	Output muscle force (N)	<b>6.32</b>	<b>0.04</b>	0.06	0.82	0.83	0.38	0.16	0.70
	Mechanical Efficiency	<b>9.31</b>	<b>0.02</b>	1.31	0.27	3.26	0.10	0.01	0.91
	Strain Energy (Bite; J)	3.81	0.09	0.33	0.57	0.03	0.87	2.17	0.18
	Model Volume (mm <sup>3</sup> )	0.04	0.86	0.06	0.81	0.77	0.40	0.19	0.68
	Jaw length (mm)	1.45	0.26	1.12	0.30	2.12	0.17	0.43	0.53
	Jaw depth (mm)	<u>4.76</u>	<u>0.06</u>	1.13	0.30	<u>4.02</u>	<u>0.07</u>	0.39	0.55